A framework for Interpreting Variable Penetration Rate CPTu Tests in Mine Tailings

Jorge Macedo[1] and Renzo Cornejo[2]

[1]School of Civil and Environmental Engineering, Georgia Institute of Technology. Email: jorge.macedo@ce.gatech.edu

[2]School of Civil and Environmental Engineering, Georgia Institute of Technology

ABSTRACT

Cone penetration testing with pore pressure measurements (CPTu) is widely used in tailings engineering, with most interpretation methods formulated for fully drained or undrained responses. However, mine tailings often exhibit partially drained behavior, posing significant interpretation challenges as limited efforts have investigated this response. This study advances the understanding of partially drained responses in mine tailings by conducting variable penetration rate CPTu tests (0.2 cm/s to 15 cm/s) in a tailings storage facility (TSF). Complementary field and laboratory tests — including shear wave velocity measurements, vane shear testing, and triaxial testing — further support the assessments. A salient aspect of the evaluated TSF is its use of both conventional and thickened tailings, enabling comparisons across different depositional methods. The study highlights key interpretation challenges, particularly the uncertainties in defining drained and undrained responses. Notably, conventional tailings exhibit greater variability due to their higher susceptibility to segregation and layering, leading to a broader range of partially drained responses than thickened tailings. A framework that integrates numerical simulations of the CPTu penetration process and laboratory testing is presented to address the highlighted challenges and to constrain parameters of interest, such as the tailings' state and the operative coefficient of consolidation. The framework's application is showcased using the collected information.

INTRODUCTION

Cone penetration testing with pore pressure measurements (CPTu) is widely used in tailings engineering. Conventionally, the CPTu test consists of pushing a 10 cm^2 or 15 cm^2 probe at a standard rate of 2 cm/s. At this rate, penetration is expected to produce fully drained responses (i.e., immediate dissipation of excess pore pressures) in sandy materials with high hydraulic conductivity and fully undrained responses (i.e., no dissipation of excess pore pressures) in clayey materials with low hydraulic conductivity. However, the response of intermediate materials, such as mine tailings, is more complex. Whether they behave in a drained, undrained, or partially drained manner during CPTu penetration depends on multiple factors, including cone geometry, penetration rate, and mechanical properties (Oliveira et al. 2011; DeJong et al. 2012; Dienstmann et al. 2018; Ayala et al. 2023). The distinctive mechanical properties of mine tailings further complicate their penetration response (e.g., Macedo and Vergaray 2022).

This study presents insights from variable rate CPTu testing conducted at an active TSF where two distinct types of mine tailings — conventional and high-density thickened tailings (hereinafter referred to as thickened tailings) — are deposited, providing a unique opportunity to examine penetration rate effects across different depositional methods. These materials exhibit contrasting solid contents, typically 25–40% for conventional tailings and 40–65% for thickened tailings, which influence their penetration response. Conventional tailings tend to form large ponds, undergo greater segregation (Watson et al. 2010), and deposit under different energy conditions compared to thickened tailings (Reid and Jefferies 2018; Macedo et al. 2024). The study specifically addresses the challenges of interpreting drained and undrained conditions in the investigated TSF and introduces a framework that integrates experimental testing and numerical simulations to analyze variable-rate CPTu data. Field-scale studies on variable rate CPTu testing in mine tailings remain scarce (as discussed in the next section), highlighting this study's contribution to improving the understanding of tailings response under varying penetration rates and drainage conditions.

PREVIOUS STUDIES

Several studies have investigated variable-rate CPTu tests and partially drained responses, primarily focusing on natural soils. These efforts include research on sandy materials (Krage et al. 2014b; Suzuki and Lehane 2015; Martinez et al. 2016b; Chow et al. 2018; Tian and Lehane 2022), clayey materials (Lehane et al. 2009; Sheng et al. 2014; Ceccato et al. 2016; Ceccato and Simonini 2017; Orazalin and Whittle 2018), clay-sand mixtures (Kim et al. 2008; Jaeger et al. 2010; Salgado and Prezzi 2014; Doan and Lehane 2018), and silts (Martinez et al. 2016a; Martinez et al. 2016b; Price et al. 2019; Zhang et al. 2022). Most of these studies have been conducted in controlled environments, such as centrifuge tests (Lehane et al. 2009; Jaeger et al. 2010; Chow et al. 2018; Orazalin and Whittle 2018; Price et al. 2019; Zhang et al. 2022) and calibration chamber tests (Kim et al. 2008; Salgado and Prezzi 2014; Doan and Lehane 2018; Tian and Lehane 2022), with fewer investigations conducted at the field scale (Kim et al. 2008; Martinez et al. 2016a; Orazalin and Whittle 2018). Some studies have also incorporated numerical simulations, primarily using analytical models such as cavity expansion (Sheng et al. 2014; Suzuki and Lehane 2015; Orazalin and Whittle 2018; Zhang et al. 2022). More recent efforts have employed advanced numerical frameworks capable of simulating large deformations in the penetration process, such as the material point method (MPM) (Ceccato et al. 2016; Ceccato and Simonini 2017; Yost et al. 2022) and the particle finite element method (PFEM) (Monforte et al. 2021; Oliynyk et al. 2022).

Previous efforts have introduced the backbone rate effect curve concept to interpret variable-rate penetration data. These curves relate normalized CPTu responses to a normalized penetration rate, typically defined as $V_h = vd/c_h$, where v is the penetration rate, d is cone diameter, and c_h is the horizontal coefficient of consolidation. Figure 1 illustrates this concept using normalized CPTu tip resistance $Q = (q_t - \sigma_v)/\sigma'_v$, where q_t is the CPTu corrected tip resistance, and σ_v and σ'_v are the total and effective vertical stresses. In loose contractive materials, Q reaches a maximum value, Q_D, under drained conditions at low

V_h, and a minimum value, Q_U, under undrained conditions at high V_h. The opposite trend occurs in dilative materials (e.g., Ayala et al. 2023). In natural soils, drained conditions typically correspond to V_h values below 0.1-0.3, while undrained conditions occur at V_h exceeding 30-100 (Randolph and Hope 2004; Schnaid 2005; DeJong and Randolph 2012); The ratio Q_D/Q_U generally ranges from 2 to 6 for clayey soils with greater variability in silty materials (DeJong et al. 2012).

Compared to natural soils, previous efforts investigating CPTu rate effects in mine tailings remain limited. Oliveira et al. (2011) proposed a physics-based analytical model to estimate backbone rate effect curves and applied it to silty tailings data obtained from variable-rate penetration tests using a 0.9 mm miniature cone in centrifuge experiments. Their results indicate that the ratio of drained tip resistance, $q_{t,D}$, to undrained tip resistance, $q_{t,U}$ varies from 3 to 4, with the transition from undrained to partially drained conditions occurring at $V_h = 50$. Although not explicitly stated, interpreting their data suggests that the transition to a fully drained response occurs at $V_{=}0.5$. Dienstmann et al. (2018) analyzed variable-rate CPTu data from the Fazenda Brasileiro TSF in Brazil. Their findings suggest partially drained conditions in the range of $V_h = 0.01$ to 10. Using a poroelastic analytical solution and CamClay simulations, they highlighted that the Q_D/Q_U ratio (approximately 11 for their materials) is primarily influenced by stiffness and strength. However, their tip resistance simulations differ significantly from the field data, likely due to complexities in the field and modeling limitations. Schnaid et al. (2020) introduced an alternative normalization for penetration velocity, defined as $\overline{V}_h = vt_{50}/(d\sqrt[4]{I_r})$ where t_{50} represents the time to reach 50% consolidation in dissipation tests and $I_r = G/Su$ is the rigidity index defined based on the operative shear modulus (G) and the undrained shear strength (Su). They applied this approach to data from Sosnoski (2016), collected at the same TSF investigated by Dienstmann et al. (2018). The motivation for this normalization was to mitigate uncertainties introduced by c_h. Despite analyzing the same TSF, Schnaid et al. (2020) reported a Q_D/Q_U ratio of approximately 20, contrasting with the value of 11 reported by Dienstmann et al. (2018).

This suggests substantial Q_D/Q_U variability even within the same TSF or that the significant scatter in the two datasets influenced the reported ratios. Notably, the Q_D/Q_U values they reported are significantly higher than those typically observed in natural soils, which rarely exceed six (DeJong and Randolph 2012). More recently, Dienstmann et al. (2024) combined Monte Carlo simulations and cavity expansion analyses to assess the variability in backbone rate effect curves using data from the same TSF examined by Dienstmann et al. (2018) and Schnaid et al. (2020). Additionally, Ayala et al. (2023) proposed a method for estimating the state parameter ψ (Been and Jefferies 1985) in partially drained conditions by integrating cavity expansion simulations using the NorSand model (Jefferies 1993) with backbone rate effect curves.

SITE INVESTIGATIONS

The investigated site is the TSF of a gold mine that has been producing and depositing tailings since the 1990s. Throughout its operation, the TSF has stored two types of tailings: conventional tailings from 1990 to 2010 and thickened tailings thereafter. The conventional tailings were deposited with a solid content of approximately 50%, while the thickened tailings had a higher solid content of around 72%. Figure 2 presents the particle size distribution for collected samples of both tailings types. The thickened tailings exhibit a narrower range due to their reduced segregation tendencies. Both conventional and thickened tailings classify as low-plasticity silts, with fine contents (FC) generally exceeding 70% and plasticity indices (PI) ranging from 0% to 2%. Table 1 summarizes representative index properties for the examined tailings.

The field investigations included CPTu tests with shear wave (V_s) and compression wave (V_p) velocity measurements as well as dissipation tests. The CPTu tests were conducted at the standard penetration rate of 2 cm/s and at non-standard rates of 0.2, 10, and 15 cm/s, following the layout shown in Figure 3. Vane shear testing supplemented the CPTu tests, and borehole samples were recovered for triaxial testing, which will be discussed later. Variable rate CPTu tests (designated as CPTu02, CPTu10, and CPTu15) were conducted within

1.5 m of the central standard CPTu (CPTu2). The numerical values in the CPTu labels correspond to the penetration rates, e.g., CPTu02 refers to a penetration of 0.2 cm/s. The spacing between CPTu tests was kept below half of the average horizontal correlation length of the deposited tailings (both conventional and thickened), which Macedo et al. (2024) estimated at approximately 3.2 m based on 15 additional standard CPTu tests conducted for spatial variability assessment.

General characterization and response at the standard CPTu penetration rate

Figure 4 presents the CPTu responses from the standard penetration push (CPTu2), which extended to a depth of 20 m. The corrected tip resistance, q_t, sleeve friction, f_s, and excess pore pressure, u_2, distinguish the boundary between conventional and thickened tailings at approximately 8.8 m, with thickened tailings overlaying the conventional deposit. The first 2 m corresponds to an access pad, so this data is not shown. Figure 4 also includes the variation of V_s, V_p, and the soil behavior type index (I_c) proposed by Robertson (2016). I_c is estimated as $I_c = \sqrt{(3.47 - \log Q_{tn})^2 + (\log F_r + 1.22)^2}$, where $Q_{tn} = \frac{(q_t - \sigma_v)}{P_a}\left(\frac{P_a}{\sigma'_v}\right)^n$ is the normalized tip resistance, $F_r = \frac{f_s}{(q_t - \sigma_v)} \times 100\%$ is the normalized friction ratio, P_a is the atmospheric pressure, and $n = 0.381 I_c + 0.05\left(\frac{\sigma'_v}{P_a}\right) - 0.15$. The figure also presents normalized CPTu responses, the modified Soil Behavior Type index, I_B, proposed by Robertson (2016), defined as $I_B = 100(Q_{tn} + 10)/(70 + Q_{tn} F_r)$, and the CPTu chart proposed by Robertson (2016) with the collected data. The endpoints of the dissipation tests, marked as circles in the pore pressure plot of Figure 4, indicate a groundwater level at 6 m. A similar interpretation applies to dissipation tests from other CPTu locations not shown in the figure.

V_p transitions to values indicative of full saturation ($V_p > 1500$ m/s) at approximately 7.5 m. Since V_p is highly sensitive to small variations in saturation, this suggests that materials between 6.0 and 7.5 m are likely to be nearly but not fully saturated. V_s values, around 200 m/s, indicate relatively soft materials, which is expected for mine tailings. The thickened tailings exhibit q_t values below 5 Mpa and f_s values under 50 kPa, with relatively uniform characteristics (as observed in the F_r variation), particularly below 5 m. This uniformity is consistent with their non-segregating nature. I_c values range from 1.8 to 2.6, suggesting the materials behave as sandy silt and silty sand mixtures, with the Robertson (2016) chart classifying them primarily as contractive sand-like and transitional. The conventional tailings exhibit higher q_t (generally between 5 and 10 MPa) and higher f_s (typically 50 to 100 kPa) compared to the thickened tailings. Their more segregating nature results in greater fluctuations in q_t and f_s, which is also reflected in more F_r variations. I_c remains below 2.5 in most of the profile, except for some layers where it reaches values up to 3.1. The conventional tailings predominantly behave as sands to silty sands; the Robertson (2016) chart classifies them as contractive sand-like and transitional, with some dilative lenses.

Responses in variable rate CPTus

Figure 5 compares the q_t, f_s, and u_2 data collected from the variable rate CPTus (CPTu02, CPTu10, CPTu15) with the standard CPTu (CPTu2). Within the thickened tailings, q_t in CPTu02 is approximately 4 MPa, exceeding the values recorded in the CPTus pushed at higher penetration rates. q_t in CPTu10 and CPTu15 remains similar, around 2.5 MPa, indicating that undrained conditions likely occur at penetration rates exceeding 10 cm/s. The slowest CPTu (CPTu02) records the lowest u_2 among the four CPTus but does not align with the hydrostatic pore pressure profile, suggesting that thickened tailings have not yet reached fully drained conditions at 0.2 cm/s. The u_2 in CPTu10 and CPTu15 are generally lower than those in CPTu2, suggesting that viscosity effects may have influenced pore pressures at high penetration rates; consistent with observations by (Wroth 1984; Lehane et al. 2009; Chow et al. 2018).

In the conventional tailings (below 8.8 m), the responses are more complex due to their greater segregation and variability. However, a general trend of decreasing q_t with increasing penetration rate is still observed. At some depths, such as around 9.5 m q_t in the standard CPTu closely matches that of the slow CPTu (CPTu02), suggesting that drained conditions may have been achieved at the standard and lower penetration rates. The q_t values for CPTu10 and CPTu15 vary at certain depths, making the assessment of undrained conditions more challenging compared to thickened tailings. The u_2 values of the slow CPTu02 generally converge to the hydrostatic pore pressure profile, suggesting that the conventional tailings exhibit drained behavior at this push rate. u_2 generally increases as the pushing rate increases up to 10 cm/s, after which it tends to decrease. As discussed previously, this reduction may be linked to viscosity effects at higher penetration rates.

Dissipation tests and c_h estimation

Estimating V_h requires calculating c_h, which depends on t_{50} and $Ir = G/Su$, where G is the operative shear modulus that can be linked to G_{max}. We estimate t_{50}, G_{max}, and Su using dissipation tests, CPTu-based shear wave velocity measurements, triaxial tests on recovered samples, and vane shear tests.

Dissipation tests were conducted at regular intervals on all CPTUs. Figure 6 presents normalized excess pore pressure dissipation curves below the groundwater level, plotted as $\Delta u_2/u_{2,max}$ versus time, where Δu_2 represents excess pore pressure and $u_{2,max}$ is the maximum excess pore pressure recorded during dissipation. The curves are shown as a function of penetration rate (excluding 0.2 cm/s CPTus, as their initial pore pressure was close to hydrostatic) for tests conducted on thickened and conventional tailings. For the standard CPTu pushed at 2 cm/s, the dissipation curves for both thickened and conventional tailings fall within a relatively narrow range. In contrast, the curves show more variability for the CPTus pushed at 10 cm/s and 15 cm/s, particularly in the conventional tailings, likely due to their higher heterogeneity. The dissipation curves for the higher penetration rates decay more rapidly, suggesting partial consolidation effects in the standard 2 cm/s CPTu. Similar behavior was observed by DeJong et al. (2012) in cavity expansion analyses conducted by Silva et al. (2006) and experimental data on Kaolin from Schneider et al. (2007). This phenomenon occurs because partial consolidation during penetration slows the subsequent dissipation of pore pressure, leading to an overestimation of t_{50} compared to interpretations assuming fully undrained penetration, as also noted in the Silva et al. (2006) and Schneider et al. (2007) datasets. Since the fastest penetration rates are expected to induce undrained conditions, the dissipation curves from these tests serve as the basis for t_{50} interpretation. Figure 6 indicates t_{50} ranging from 3 to 7 s in the thickened tailings and 1 to 8 s in the conventional tailings, with the lower range corresponding to the sandier units.

Figure 7a presents the results of vane shear tests conducted at a rotation rate of 0.1 degrees/s on both thickened and conventional tailings. The tests indicate that Su values range from 50 to 70 kPa in the thickened tailings and from 40 to 110 kPa in the conventional tailings. Figure 7b shows the Su/σ' ratio estimated from laboratory triaxial tests, suggesting a consistent value of 0.2 for both thickened and conventional tailings. Section 4 provides a more detailed discussion of the available triaxial test results, and supplemental material A shows the interpretation of the strength ratios.

Figure 8 compares Su values estimated from vane shear and triaxial tests with those derived from CPTu data using $Su = (q_t - \sigma_v)/N_{kt}$ and the CPTu pushed at 15 cm/s. An operational $N_{kt} = 18$ is selected because it allows a reasonable consistency between vane shear and CPTu-based estimates. The potential range of Su values from vane shear, laboratory, and CPTu will be used in subsequent analyses. Figure 8 presents the variation of G_{max}, estimated from the measured V_s values using $G_{max} = \rho V_s^2$, where ρ is the density derived from CPTu data using the Robertson and Cabal (2022) correlation. The average G_{max} values for thickened and conventional tailings are 65 MPa and 100 MPa, respectively. A curve fitting the G_{max} data, $G_{max} = 60[p'/P_a]^{0.7}$, where p' is the mean effective stress, is also included.

Using the plausible variations in Su and G_{max}, the G_{max}/Su ratio is estimated at depths where dissipation tests were conducted, with results shown in Figure 8d. Estimates also consider the Krage et al. (2014b) procedure, which uses an operative G. To evaluate G_{max}/Su, the estimates were scaled by a factor of 3.84, following Krage et al. (2014b). The results indicate. The results indicate G_{max}/Su values ranging from 50 to 3000, with no significant distinction between thickened and conventional tailings.

c_h is evaluated using t_{50} estimates at each depth and two approaches: Teh and Houlsby

(1991) with $c_h = 0.245a^2\sqrt{I_r}/t_{50}$, and Mayne et al. (2023) with $c_h = 0.028a^2{I_r}^{0.75}/t_{50}$. Since the operative I_r in Teh and Houlsby (1991) is typically based on the secant shear modulus, G_{50} (Krage et al. 2014a), I_r is scaled by G_{50}/G_{max}. The Mayne et al. (2023) approach considers the operative I_r based on the shear modulus at peak conditions, G_{peak}, so I_r is scaled by G_{peak}/G_{max}. G_{50}/G_{max} and G_{peak}/G_{max} are estimated from available laboratory tests (supplemental material A) and are, on average, 0.45 and 0.26 for thickened tailings and 0.30 and 0.19 for conventional tailings. Figure 8e presents the resulting c_h variations.

Assessment of rate effects and uncertainties

Using the previously discussed c_h estimates, Q backbone rate effect curves can now be constructed. Figure 9 presents these curves at different depths for both thickened and conventional tailings, using average c_h values. Following Dienstmann et al. (2018), Q values at each depth are computed as the average over 10 cm intervals. The analysis for thickened tailings focuses on the 6.0 m to 8.8 m depth interval (Figure 9a), which lies below the groundwater table. Conventional tailings exhibit greater variability; hence, different layers are analyzed based on the F_r variation (Figure 4). The considered depth intervals are: 8.8 – 9.8 m (Figure 9b), 9.8 – 12.2 m (Figure 9c), and 12.2 – 13.0 m (Figure 9d). Depths below 13 m are excluded since the slow CPTu at 0.2 cm/s did not reach those depths. At depths with significant layering, such as 9.8 – 12.2 m, increased variability in Q is observed. However, the expected trend of decreasing Q with increasing $V_h = 0.1$ remains. In more homogeneous depths, particularly within thickened tailings, the backbone rate effect curves exhibit clearer trends.

Empirical upper and lower boundaries are included using the DeJong et al. 2012 formulation, which estimates Q using $Q/Q_U = 1 + (Q - Q_U)/(1 + (V/V_{50})^c)$, where V_{50} and c are fitting parameters and the remaining variables are as defined before. Figure 9 shows the estimated upper and lower boundaries. A distinct trend emerges in the drained and undrained behavior of the two tailings types. In thickened tailings, the definition of drained conditions remains uncertain, while in conventional tailings, there is more uncertainty in determining undrained conditions, particularly in the depth intervals of 8.8 - 9.8 m and 12.2 - 13.0 m. At a penetration rate of 0.2 cm/s, conventional tailings reach drained conditions at $V_h = 0.1$, but achieving fully undrained conditions may require $V_h > 10$, which exceeds the fastest CPTu penetration rate used. In contrast, thickened tailings require lower penetration rates,$V_h < 0.1$, than the slowest CPTu to reach drained conditions, while undrained conditions occur at V_h of about 30, corresponding to the fastest penetration rate. Representative depths at 7.35 m (thickened tailings) and 12.60 m (conventional tailings) are selected to further illustrate uncertainties. Figure 10 presents backbone curves derived using the DeJong et al. (2012) functional form. In thickened tailings, various combinations of V_{50} and c are possible for the collected data, leading to uncertainties in Q_D and Q_D/Q_U as Figure 10a shows. For conventional tailings, a range of Q_U values (2 to 10), informed by Figure 9, produces backbone curves that align well with the collected data, suggesting a plausible Q_D/Q_U ratio between 2.5 and 10, as illustrated in Figure 10b.

INTERPRETATIONS INTEGRATING NUMERICAL SIMULATIONS AND LABORATORY TESTING

This section presents a framework that incorporates numerical simulations of the CPTu penetration process to aid in interpreting variable penetration rate CPTus when uncertainties exist in reaching drained or undrained conditions. Figure 11 outlines the general framework and its sequential steps. Step 1 has already been addressed in the previous section, which highlights the uncertainties in defining drained or undrained responses. The following subsections will demonstrate Steps 2 to 4 using the collected data and representative depths at 7.35 m for the thickened tailings and 12.60 m for the conventional tailings.

CPTu penetration modeling and constitutive model

We conduct numerical simulations with a focus on large deformations using the geotechnical particle finite element method (G-PFEM). G-PFEM has been applied in various geotechnical problems, including granular flow, landslides, and contact problems (e.g., Zhang et al. 2013; Cante et al. 2014; Cremonesi et al. 2011; Franci et al. 2020; Ciantia 2024; Monforte et al. 2017b; Previtali et al. 2023), as well as CPTu penetration simulations (Monforte et al. 2021; Oliynyk et al. 2022; Ciantia et al. 2022). Cremonesi et al. (2020) provide a detailed comparison between G-PFEM and the traditional finite element method (FEM). Unlike FEM, G-PFEM treats nodes as "particles" that act as discrete material points carrying information on velocity, displacement, and stress. These particles dynamically update the mesh using different re-meshing boundary condition treatment techniques, such as Delaunay Tessellation and the alpha-shape method (Cremonesi et al. 2020). We use the G-PFEM implementation in the multiphysics platform Kratos (Monforte et al. 2017a) with the GiD package (Ribó et al. 1998) for pre- and post-processing. G-PFEM can accommodate advanced constitutive models; we use CASM (Clay and Sand Model) initially proposed by Yu (1998), which has been previously used in several CPTu penetration-focused efforts (Monforte et al. 2021; Monforte et al. 2023; Boschi et al. 2024). Figure 12 illustrates the key features of CASM in the p'-ν and p'-q spaces, where $\nu = e + 1$ is the specific volume, with e being the void ratio. The supplemental material B provides a summary of CASM's constitutive equations. CASM extends the Cam Clay model (Roscoe and Burland 1968) by incorporating the state parameter (ψ, Been and Jefferies 1985). The model defines a reference consolidation line (RCL) parallel to the critical state line (CSL), separated by a distance r. The CSL has a slope λ and an altitude Γ (Figure 12a). The RCL corresponds to a reference state parameter (ψ_r), which relates to r as $\psi_r = (\lambda - \kappa)\ln r$, where κ is the recompression curve slope. The yield surface shape in p'-q space is controlled by parameter n (Figure 12b), and the CSL in this space has a slope M_{tc} for triaxial compression conditions. A hardening law similar to that of the Cam Clay model governs the evolution of the yield surface (supplemental material B), which depends on the initial mean pressure (p'_0), the initial specific volume (ν_{init}), λ, and κ. Plastic volumetric strain generation is controlled by a non-associative flow rule and the constitutive parameter m. Elasticity is characterized by G and the bulk modulus K, which can be estimated from κ as in Cam Clay. CASM parameters include Γ, λ, κ, M_{tc}, n, r, and G, all of which can be calibrated from experimental tests. Additionally, forward predictions require the initial state parameter ψ_0, estimated as $\psi_0 = \nu_{init} - \Gamma + \lambda \ln(p')$. The next section discusses the calibration of the required parameters based on the available testing.

Laboratory testing and model calibration

The CASM parameters are calibrated using triaxial test data for both thickened and conventional tailings. The testing program includes seven triaxial tests on thickened tailings (Figure 7a) and five tests on conventional tailings (Figure 7b). The supplemental material A provides additional details on the triaxial tests. Using the terminology from Macedo and Vergaray (2022), the undrained response in thickened tailings varies from partial softening, where q decreases after peak to a nonzero value (observed in TXCU1 and TXCU2), to limited flow, where the response transitions from contractive to dilative after significant shearing (observed in TXCU3). The drained responses exhibit hardening, where q increases monotonically in initially loose samples with a positive initial ψ (TXCD1 and TXCD2). In contrast, initially dense samples (negative initial ψ) show a peak in q, indicative of maximum dilation, followed by softening. Conventional tailings exhibit similar response patterns, but all tests were conducted on initially loose samples, placing them above the CSL (Figure 7b). The critical state lines (CSLs) in the $p' - e$ and $p' - q$ spaces are estimated by fitting the test endpoints, yielding λ, Γ, and M_{tc} values summarized in Table 2, which are directly used as CASM parameters. The initial pre-shearing states of both tailings are used to estimate the reference consolidation lines (RCLs), from which ψ_r values of 0.1 (thickened tailings) and 0.09 (conventional tailings) are obtained. These values are used to estimate r. The calibration of n, m, and G follows an iterative forward approach, where parameter adjustments are made by comparing experimental and numerical responses. This approach is commonly used in constitutive model calibration (e.g., Shuttle and Jefferies 2016). Table 2 summarizes the final calibrated CASM parameters. Figures 7a and b compare the experimental results with CASM numerical simulations, showing that the simulations reproduce the experimental patterns and are considered satisfactory. The calibrated parameters will be used for CPTu penetration simulations.

CPTu penetration simulations and constraining of backbone rate effect curves

The CPTu penetration process is simulated using the axisymmetric mesh shown in Figure 14, following procedures similar to those described by Monforte et al. (2018) and Monforte et al. (2021). The mesh dimensions are 0.66 m by 1.31 m, corresponding to 30 and 60 times the radius (R) of a 15 cm^2 cone. Boundary conditions constrain radial displacements (u_r) at the lateral boundaries and both radial and vertical displacements (u_y) at the bottom boundary. Pore pressures (u_w) are also fixed at the bottom boundary to prevent excess pore pressure generation. The cone is treated as a rigid body, and its interaction with the soil is modeled using a contact model based on the penalty method (Wriggers and Laursen 2006). Normal stresses develop as part of the contact model, while tangential stresses are computed using procedures outlined by Wriggers (1995) and Wriggers and Laursen (2006), with slip-yield conditions following Monforte et al. (2018). This contact model has been widely applied in previous CPTu penetration studies (e.g., Monforte et al. 2021), and further details can be found in Monforte et al. (2018). The mesh discretization employs linear triangular elements, with refinement in the region surrounding and beneath the cone (extending approximately 25R) using an average element size of 4 mm. Element sizes increase further from the cone's influence zone, reaching approximately 50 mm near the boundaries. Vertical stresses are initialized based on the in situ stress conditions at the analyzed depths (7.35 m for thickened tailings and 12.60 m for conventional tailings) by applying a distributed vertical load at the top boundary. Horizontal stresses are initialized, assuming a K_0 value of 0.70. At the start of the simulation, the cone is embedded at a depth of $10R$, after which the penetration simulation begins. Following the methodology of Monforte et al. (2021), Ceccato et al. (2016), and Ceccato and Simonini (2017), the cone advances at a constant velocity of 2 cm/s in all simulations. However, hydraulic conductivity is varied across six orders of magnitude, ranging from 10^{-5} to 10^{-10} cm/s, to simulate drained and undrained conditions. Consistent with Monforte et al. (2018), the mesh refinement criterion is governed by plastic shear strain evolution. When an element exceeds a plastic shear strain of 0.01%, additional nodes are introduced, and node information is updated accordingly.

Figure 15 presents typical contours of mean stresses, deviatoric stresses, and excess pore pressures under drained, partially drained, and undrained conditions for thickened tailings, using $\psi_0 = 0.025$ and the parameters in Table 2 for illustration. The drained simulations produce negligible excess pore pressures, whereas excess pore pressures increase within the cone's influence zone as the response transitions to undrained conditions. Mean stresses are higher in drained simulations and decrease near the cone as the response becomes more undrained. Conversely, deviatoric stresses follow an inverse trend, increasing as the response transitions from undrained to drained. The response patterns in conventional tailings follow similar trends and are omitted for brevity. Overall, the results qualitatively align with variable rate CPTu simulations from previous studies (e.g., Monforte et al. 2021; Oliynyk et al. 2022). Figure 16 illustrates the typical variation of Q extracted from numerical simulations using the same input parameters while varying hydraulic conductivity (k) between 10^{-5} and 10^{-10} cm/s. The results for both thickened and conventional tailings show that as k increases (i.e., V_h decreases), Q approaches Q_D, and as k decreases (i.e., V_h increases), Q approaches Q_U.

The missing parameter needed to estimate backbone rate effect curves is ψ. We propose an iterative procedure to determine ψ: (1) select ψ range and conduct simulations for drained or undrained conditions using the upper and lower bounds of the selected range; (2) compare the numerically obtained Q_D or Q_U with field-measured values; (3) interpolate to update ψ based on the difference between numerical and field values of Q_D or Q_U from step 2; and (4) repeat steps 1 to 3 until the numerical Q_D or Q_U matches the field values, defining ψ as the value that achieves this match. Figure 17 illustrates this procedure. For the thickened tailings, we use Q_U because undrained conditions are reached at the fastest penetration rate, as previously discussed. The initial ψ range is set between 0.00 and 0.05, and simulations at $\psi = 0.00$ and $\psi = 0.05$ define the range indicated by the horizontal arrow at 7.35 m in Figure 17. Based on the difference between the numerical and field Q_U, the next iteration interpolates $\psi = 0.025$; the numerically updated Q_U now matches the field Q_U and is therefore selected. For the conventional tailings, we follow the same procedure but use Q_D since drained conditions are reached in the field. The initial ψ range is again set between 0.00 and 0.05, with Q_D results indicated by the horizontal arrow at 12.60 m in Figure 17. Coincidentally, ψ is also estimated as 0.025 at this depth. Using the estimated ψ values at each depth and the calibrated parameters in Table 2, we proceed with numerical simulations across a range of V_h values to construct the backbone rate effect curves.

The c_h required to estimate V_h from numerical simulations is Monforte et al. (2021):

$$c_h = \frac{\sigma'_{v0}(1+e_0)k}{\lambda\gamma_w}$$

where γ_w is the water unit weight, and the remaining variables are as previously defined. This expression implies that c_h is governed by conditions along the virgin compression curve. An alternative approach replaces λ with κ, in which case c_h reflects conditions along the recompression line, where elasticity is typically assumed (Mahmoodzadeh et al. 2014). Given the complex stress conditions when the CPTu penetrates, Mahmoodzadeh et al. (2014) recommends using an operative c_h, which accounts for both λ and κ according to:

$$c_{op} = \frac{1-\mu}{1+\mu}\frac{(1+2K_0)\sigma'_{v0}(1+e_0)k}{\lambda^{(1-\alpha)}\kappa^{\alpha}\gamma_w}$$

where μ is the Poisson ratio, and α represents the tradeoff between λ and κ in controlling compressibility effects. Figure 18 presents backbone rate effect curves using operative c_h values derived from λ, κ, and the λ-κ tradeoff, following Mahmoodzadeh et al. (2014) with $\alpha = 0.5$, $\mu = 0.3$, and $K_0 = 0.7$. The numerical simulations estimate Q, while V_h is computed as $V_h = vd/c_h$. The curves based solely on λ and κ establish upper and lower boundaries, respectively, with the λ-κ tradeoff curve positioned between them, closer to the κ-based curve. The experimental backbone curves at 7.35 m (thickened tailings) and 12.60 m (conventional tailings) are shown in Figure 18, considering the variation of field-based c_h from Figure 8e and the Q range (estimated as the variation within 10 cm). The experimental curve shapes at low and high V_h are guided by the numerical simulations for the thickened and conventional tailings, respectively. These simulations constrain Q_D for the thickened tailings and Q_U for the conventional tailings and the range of field backbone rate effect curves, which aids in identifying the operative field c_h. For instance, in the thickened tailings at 7.35 m depth, numerical simulations constrain c_h within 1.25–2.50 cm^2/s, while in the conventional tailings at 12.6 m, the field c_h is constrained to 4.25–8.50 cm^2/s. The results also suggest that partially drained conditions occur for V_h between 1–30 in the thickened tailings and 2–200 in the conventional tailings. The estimated Q_D/Q_U ratios are 3.2 for the thickened tailings and 3.0 for the conventional tailings. The framework discussed in this section provides a systematic approach to constraining Q_D/Q_U, ψ, operative c_h, and the range of partially drained responses, particularly when uncertainty exists regarding whether drained or undrained conditions are achieved in the field.

CONCLUSIONS

This study utilized variable rate CPTu tests (ranging from 0.2 cm/s to 15 cm/s), complemented by laboratory testing and additional field data from a TSF containing two distinct tailings types (thickened and conventional), to advance the understanding of partially drained responses in mine tailings. Previous field-scale studies on partially drained responses in mine tailings are scarce and, to the best of our knowledge, have been limited to the Fazenda Brasileiro TSF in Brazil. Expanding case studies of variable rate CPTu tests on mine tailings, as done in this study, is encouraged and would complement similar ongoing efforts in natural silts (e.g., Paniagua et al. 2021).

The results highlight greater variability in backbone rate effect curves for conventional tailings, leading to more uncertainties in assessing partially drained responses compared to thickened tailings. This increased uncertainty stems from the more segregating nature and layering in conventional tailings, which are directly linked to their deposition process. Additionally, the findings underscore challenges in interpreting drained and undrained responses at the examined CPTu penetration rates. These challenges are associated with (1) the variability in key parameters such as I_r and c_h, which affect partially drained responses, and (2) the penetration rates achievable in the field.

This study introduced a framework that integrates numerical simulations of CPTu penetration with laboratory testing to support the interpretation of variable rate CPTu data (Figure 11). The framework was demonstrated using the CASM model and G-PFEM but can also incorporate other constitutive models, such as Norsand (Jefferies and Been 2015), and alternative large deformation numerical schemes, such as MPM. We advocate for the use of critical state soil mechanics models, as they provide a balance between robustness and calibration effort and are already widely applied in tailings engineering. The Norsand model, for example, has been used in forensic investigations of recent failures, including Fundão (Morgenstern et al. 2016), Feijão (Robertson et al. 2019), and Cadia (Morgenstern et al. 2019).

We also believe that robust large deformation schemes to interpret CPTu tests like G-PFEM and MPM should be preferred over traditional approaches, such as cavity expansion, due to their advantages in simulating complex penetration processes. With the increasing availability of computational resources and advancements in large deformation numerical techniques (e.g., Ceccato et al. 2024), we advocate for their adoption in engineering practice as they can bring useful insights, as showcased in this study, to interpret partially drained CPTu responses.

DATA AVAILABILITY STATEMENT

Some or all data, models, or code that support the findings of this study are available from the corresponding author upon reasonable request.

ACKNOWLEDGMENTS

This material is based upon work supported by the National Science Foundation (NSF) under Grant No. CMMI 2145092. Any opinions, findings, conclusions, or recommendations expressed in this material are those of the author(s) and do not necessarily reflect the views of the NSF. The PRONABEC program of the Peruvian government also provided complementary support. In addition, we would like to thank ConeTec, Newmont, and WSP-Golder for supporting the site characterization efforts. Finally, we thank Prof. Jason DeJong for the discussions during the planning of the CPTu campaign for the variable penetration rate CPTus and geotechnical characterization.

REFERENCES

Ayala, J., Fourie, A., and Reid, D. (2023). “A unified approach for the analysis of cpt partial drainage effects within a critical state soil mechanics framework in mine tailings.” Journal of Geotechnical and Geoenvironmental Engineering, 149(6), 04023036.

Been, K. and Jefferies, M. G. (1985). “A state parameter for sands.” Géotechnique, 35(2), 99–112.

Boschi, K., Arroyo, M., Monforte, L., Carbonell, J. M., and Gens, A. (2024). “Coupled hydromechanical modelling of cone penetration in layered liquefiable soils.” Géotechnique, 1–15.

Cante, J., Davalos, C., Hernandez, J., Oliver, J., Jonsén, P., Gustafsson, G., and Häggblad, H.-Å. (2014). “Pfem-based modeling of industrial granular flows.” Computational particle mechanics, 1, 47–70.

Ceccato, F., Beuth, L., and Simonini, P. (2016). “Analysis of piezocone penetration under different drainage conditions with the two-phase material point method.” Journal of Geotechnical and Geoenvironmental Engineering, 142(12), 04016066.

Ceccato, F. and Simonini, P. (2017). “Numerical study of partially drained penetration and pore pressure dissipation in piezocone test.” Acta Geotechnica, 12, 195–209.

Ceccato, F., Yerro, A., and Di Carluccio, G. (2024). “Simulating landslides with the material point method: Best practices, potentialities, and challenges.” Engineering Geology, 107614.

Chow, S. H., Bienen, B., and Randolph, M. (2018). “Rapid penetration of piezocones in sand.” Cone penetration testing 2018, CRC Press, 213–219.

Ciantia, M. (2024). “Continuum (pfem) and discrete (dem) modelling of pile installation in rocks.” Annual Conference of the UK Association for Computational Mechanics., Durham University, 124–127.

Ciantia, M. O., Oliynyk, K., and Tamagnini, C. (2022). “Finite deformation modelling of cone penetration tests in saturated structured clays.” International Conference of the International Association for Computer Methods and Advances in Geomechanics, Springer, 195–202.

Cremonesi, M., Franci, A., Idelsohn, S., and Oñate, E. (2020). “A state of the art review of the particle finite element method (pfem).” Archives of Computational Methods in Engineering, 27, 1709–1735.

Cremonesi, M., Frangi, A., and Perego, U. (2011). “A lagrangian finite element approach for the simulation of water-waves induced by landslides.” Computers & Structures, 89(11-12), 1086–1093.

DeJong, J., Jaeger, R., Boulanger, R., Randolph, M., and Wahl, D. (2012). “Variable penetration rate cone testing for characterization of intermediate soils.” Geotechnical and geophysical site characterization, 4(1), 25–42.

DeJong, J. T. and Randolph, M. (2012). “Influence of partial consolidation during cone penetration on estimated soil behavior type and pore pressure dissipation measurements.” Journal of Geotechnical and Geoenvironmental Engineering, 138(7), 777–788.

Dienstmann, G., Perini, L., Meier, A. L., Ziesmann, N., and Campos, J. P. d. (2024). “Incorporating inherited variability into the drainage effect analysis of piezocone tests in gold tailings.” Proceedings of the Institution of Civil Engineers-Geotechnical Engineering, 1–32.

Dienstmann, G., Schnaid, F., Maghous, S., and DeJong, J. (2018). “Piezocone penetration rate effects in transient gold tailings.” Journal of Geotechnical and Geoenvironmental Engineering, 144(2), 04017116.

Doan, L. and Lehane, B. (2018). “Effects of partial drainage on the assessment of the soil behaviour type using the cpt." Cone Penetration Testing 2018, CRC Press, 275–280.

Franci, A., Cremonesi, M., Perego, U., Crosta, G., and Oñate, E. (2020). "3d simulation of vajont disaster. part 1: Numerical formulation and validation." Engineering Geology, 279, 105854.

Jaeger, R., DeJong, J., Boulanger, R., Low, H., and Randolph, M. (2010). "Variable penetration rate cpt in an intermediate soil." Proc., 2nd Int. Symp. on Cone Penetration Testing, Huntington Beach, CA, 2–50.

Jefferies, M. (1993). "Nor-sand: a simle critical state model for sand." Géotechnique, 43(1), 91–103.

Jefferies, M. and Been, K. (2015). Soil liquefaction: a critical state approach. CRC press.

Kim, K., Prezzi, M., Salgado, R., and Lee, W. (2008). "Effect of penetration rate on cone penetration resistance in saturated clayey soils." Journal of Geotechnical and Geoenvironmental Engineering, 134(8), 1142–1153.

Krage, C., Broussard, N., and DeJong, J. (2014a). "Estimating rigidity index (ir) based on cpt measurements." Proceedings of the 3rd International Symposium on Cone Penetration Testing, Las Vegas, Nevada, 727–735.

Krage, C. P., DeJong, J. T., and Wilson, D. W. (2014b). "Variable penetration rate cone testing in sands with fines." Geo-Congress 2014: Geo-characterization and Modeling for Sustainability, 170–179.

Lehane, B., O'loughlin, C., Gaudin, C., and Randolph, M. (2009). "Rate effects on penetrometer resistance in kaolin." Géotechnique, 59(1), 41–52.

Macedo, J. and Vergaray, L. (2022). "Properties of mine tailings for static liquefaction assessment." Canadian Geotechnical Journal, 59(5), 667–687.

Macedo, J., Vergaray, L., Liu, C., Sharp, J., Morrison, K. F., and Byler, B. (2024). "Cptu-based spatial variability assessment of thickened and conventional mine tailings." Journal of Geotechnical and Geoenvironmental Engineering, 150(10), 04024091.

Mahmoodzadeh, H., Randolph, M., and Wang, D. (2014). "Numerical simulation of piezocone dissipation test in clays." Géotechnique, 64(8), 657–666.

Martinez, M. F. G., Tonni, L., Gottardi, G., and Rocchi, I. (2016a). "Influence of penetration rate on cptu measurements in saturated silty soils." 5th International Conference on Geotechnical and Geophysical Site Characteristion (ISC'5).

Martinez, M. G., Tonni, L., and Gottardi, G. (2016b). "On the interpretation of piezocone tests in natural silt and sand mixtures." Cone Penetration Testing 2018, 3, 63–68.

Mayne, P., Cargill, E., and James, G. (2023). The Cone Penetration Test Better information Better Decisions. A CPT Design Parameter Manual, Vol. 1. ConeTec.

Monforte, L., Arroyo, M., Carbonell, J., and Gens, A. (2017a). "G–pfem: A particle finite element method platform for geotechnical applications." ALERT Geomaterials Workshop, Vol. 2017.

Monforte, L., Arroyo, M., Carbonell, J. M., and Gens, A. (2017b). "Numerical simulation of undrained insertion problems in geotechnical engineering with the particle finite element method (pfem)." Computers and Geotechnics, 82, 144–156.

Monforte, L., Arroyo, M., Carbonell, J. M., and Gens, A. (2018). "Coupled effective stress analysis of insertion problems in geotechnics with the particle finite element method." Computers and Geotechnics, 101, 114–129.

Monforte, L., Arroyo, M., and Gens, A. (2023). "A relation between undrained cptu results and the state parameter for liquefiable soils." Canadian Geotechnical Journal, 60(11), 1756–1774.

Monforte, L., Gens, A., Arroyo, M., Mánica, M., and Carbonell, J. M. (2021). "Analysis of cone penetration in brittle liquefiable soils." Computers and Geotechnics, 134, 104123.

Morgenstern, N., Jefferies, M., Van Zyl, D., and Wates, J. (2019). "Report on ntsf embankment failure." Ashurst, Australia.

Morgenstern, N., Vick, S., Viotti, C., and Watts, B. (2016). "Fundão tailings dam review panel report on the immediate causes of the failure of the fundão dam. samarco s.a., vale s.a.." New York: Cleary Gottlieb Steen & Hamilton LLP.

Oliveira, J. R., Almeida, M. S., Motta, H. P., and Almeida, M. C. (2011). “Influence of penetration rate on penetrometer resistance.” Journal of Geotechnical and Geoenvironmental Engineering, 137(7), 695–703.

Oliynyk, K., Ciantia, M. O., and Tamagnini, C. (2022). “Pfem modeling of cptu tests in saturated structured soils.” Cone Penetration Testing 2022, CRC Press, 623–629.

Orazalin, Z. Y. and Whittle, A. J. (2018). “Realistic numerical simulations of cone penetration with advanced soil models.” Cone Penetration Testing 2018, CRC Press, 483–489.

Paniagua, P., Lunne, T., Gundersen, A., L’Heureux, J., and Kåsin, K. (2021). “Cptu results at a silt test site in norway: effect of cone penetrometer type.” IOP Conference Series: Earth and Environmental Science, Vol. 710(1), IOP Publishing, 012010.

Previtali, M., Ciantia, M. O., and Riccio, T. (2023). “Numerical installation of oe piles in soft rocks within the gpfem framework.” 10th European Conference on Numerical Methods in Geotechnical Engineering, International Society for Soil Mechanics and Geotechnical Engineering, 322.

Price, A., Boulanger, R., and DeJong, J. (2019). “Centrifuge modeling of variable-rate cone penetration in low-plasticity silts.” Journal of Geotechnical and Geoenvironmental Engineering, 145(11), 04019098.

Randolph, M. and Hope, S. (2004). “Effect of cone velocity on cone resistance and excess pore pressures.” Effect of cone velocity on cone resistance and excess pore pressures, Yodogawa Kogisha Co. Ltd, 147–152.

Reid, D. and Jefferies, M. (2018). “A geological principle for the density of thickened tailings.” Paste 2018: Proceedings of the 21st International Seminar on Paste and Thickened Tailings, Australian Centre for Geomechanics, 117–126.

Ribó, R., Pasenau, M., Escolano, E., Ronda, J., and González, L. (1998). “Gid reference manual.” CIMNE, Barcelona, 27, 25.

Robertson, P. and Cabal, K. (2022). Guide to Cone Penetration Testing. P.K. Robertson Consulting, 7th edition, <https://www.cpt-robertson.com/wp-content/uploads/2024/09/cpt-

guide-7th-2024.pdf>.

Robertson, P. K. (2016). “Cone penetration test (cpt)-based soil behaviour type (sbt) classification system—an update.” Canadian Geotechnical Journal, 53(12), 1910–1927.

Robertson, P. K., De Melo, L., Williams, D., and Wilson, G. (2019). “Report of the expert panel on the technical causes of the failure of feijão dam i.” Commissioned by Vale.

Roscoe, K. H. and Burland, J. B. (1968). “On the generalized stress-strain behaviour of ’wet’ clay.” Engineering Plasticity, J. Heyman and F. Leckie, eds., Cambridge University Press, 535–609.

Salgado, R. and Prezzi, M. (2014). “Penetration rate effects on cone resistance: insights from calibration chamber and field testing.” Soils and Rocks, 233.

Schnaid, F. (2005). “Geocharacterisation and properties of natural soils by in situ tests.” Proceedings of the International Conference on Soil Mechanics and Geotechnical Engineering, 3–45.

Schnaid, F., Dienstmann, G., Odebrecht, E., and Maghous, S. (2020). “A simplified approach to normalisation of piezocone penetration rate effects.” Géotechnique, 70(7), 630–635.

Schneider, J. A., Lehane, B. M., and Schnaid, F. (2007). “Velocity effects on piezocone measurements in normally and over consolidated clays.” International Journal of Physical Modelling in Geotechnics, 7(2), 23–34.

Sheng, D., Kelly, R., Pineda, J., and Bates, L. (2014). “Numerical study of rate effects in cone penetration test.” 3rd international symposium on cone penetration testing, 419–428.

Shuttle, D. and Jefferies, M. (2016). “Determining silt state from cptu.” Geotechnical Research, 3(3), 90–118.

Silva, M. F., White, D. J., and Bolton, M. D. (2006). “An analytical study of the effect of penetration rate on piezocone tests in clay.” International journal for numerical and analytical methods in geomechanics, 30(6), 501–527.

Sosnoski, J. (2016). “Interpretation of cptu and dmt tests in intermediate permeability soils.” M.S. thesis. Universidade Federal do Rio Grande do Sul, Porto Alegre, Brazil.

Suzuki, Y. and Lehane, B. (2015). “Analysis of cpt end resistance at variable penetration rates using the spherical cavity expansion method in normally consolidated soils.” Computers and Geotechnics, 69, 141–152.

Teh, C. and Houlsby, G. (1991). “An analytical study of the cone penetration test in clay.” Geotechnique, 41(1), 17–34.

Tian, Y. and Lehane, B. (2022). “Parameters affecting the cpt resistance of reconstituted sands.” Cone Penetration Testing 2022, CRC Press, 734–740.

Watson, A., Corser, P., Garces Pardo, E., Lopez Christian, T., and Vandekeybus, J. (2010). “A comparison of alternative tailings disposal methods—the promises and realities.” Mine Waste 2010: Proceedings of the First International Seminar on the Reduction of Risk in the Management of Tailings and Mine Waste, Australian Centre for Geomechanics, 499–514.

Wriggers, P. (1995). “Finite element algorithms for contact problems.” Archives of computational methods in engineering, 2, 1–49.

Wriggers, P. and Laursen, T. A. (2006). Computational contact mechanics, Vol. 2. Springer.

Wroth, C. (1984). “The interpretation of in situ soil tests.” Geotechnique, 34(4), 449–489.

Yost, K. M., Yerro, A., Green, R. A., Martin, E., and Cooper, J. (2022). “Mpm modeling of cone penetrometer testing for multiple thin-layer effects in complex soil stratigraphy.” Journal of Geotechnical and Geoenvironmental Engineering, 148(2), 04021189.

Yu, H.-S. (1998). “Casm: A unified state parameter model for clay and sand.” International journal for numerical and analytical methods in geomechanics, 22(8), 621–653.

Zhang, J., Meng, Q., Zhang, Y., Feng, X., Wei, G., Su, X., and Liu, T. (2022). “Effect of penetration rates on the piezocone penetration test in the yellow river delta silt.” Journal of Ocean University of China, 21(2), 361–374.

Zhang, X., Krabbenhoft, K., Pedroso, D., Lyamin, A., Sheng, D., Da Silva, M. V., and Wang, D. (2013). “Particle finite element analysis of large deformation and granular flow problems.” Computers and Geotechnics, 54, 133–142.

List of Tables

TABLE 1. Average particle size distribution properties and Atterberg Limits for the conventional and thickened tailings

Property	Conventional tailings	Thickened tailings
Sand fraction (%)	28.70	24.70
Silt fraction (%)	67.70	70.90
Clay fraction (%)	3.60	4.40
Specific gravity (G_s)	3.31	3.38
Liquid limit (LL)	22	22
Plasticity index (PI)	2	2

TABLE 2. Calibrated CASM parameters for the considered thickened and conventional tailings

Parameter	Thickened tailings	Conventional tailings
Γ	2.174	2.217
λ	0.065	0.068
κ	0.032	0.034
M_{tc}	1.55	1.55
n	1.5	1.5
r	6.8	6.0
m	2.4	2.4
ψ_r	0.10	0.09
G	14 MPa	14 MPa

List of Figures

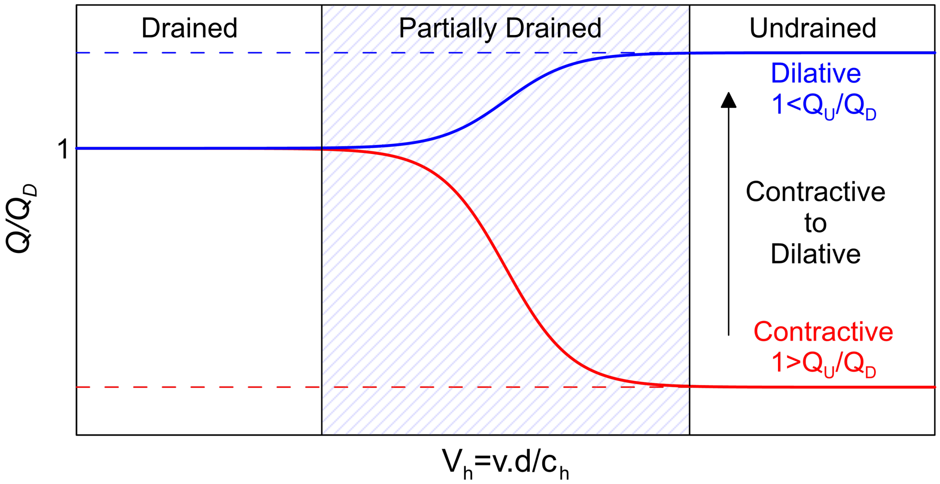

FIG. 1. Illustration of partially drained effects on contractive and dilative materials.

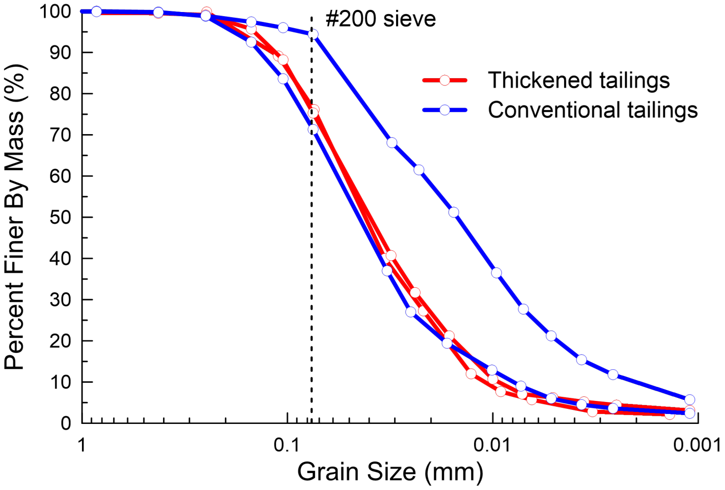

FIG. 2. Range of particle size distributions for thickened and conventional tailings.

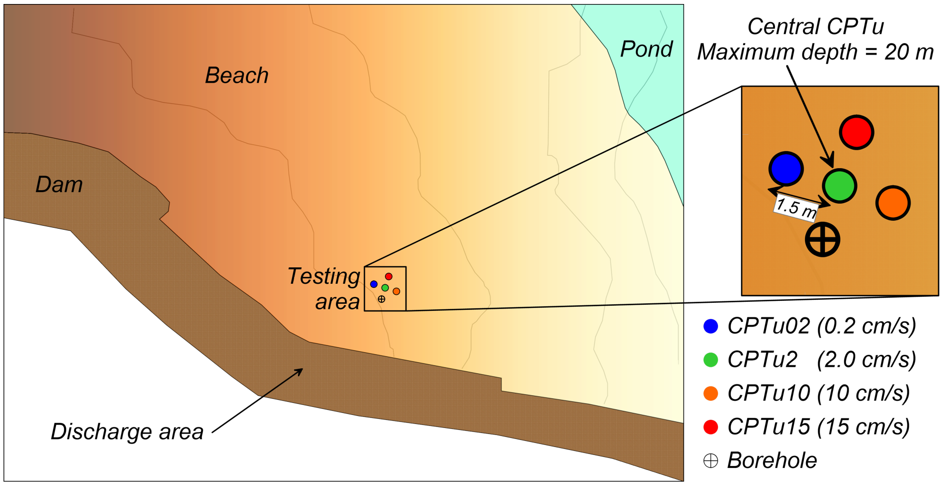

FIG. 3. Schematic representation for the location of variable penetration rate CPTus on the investigated TSF

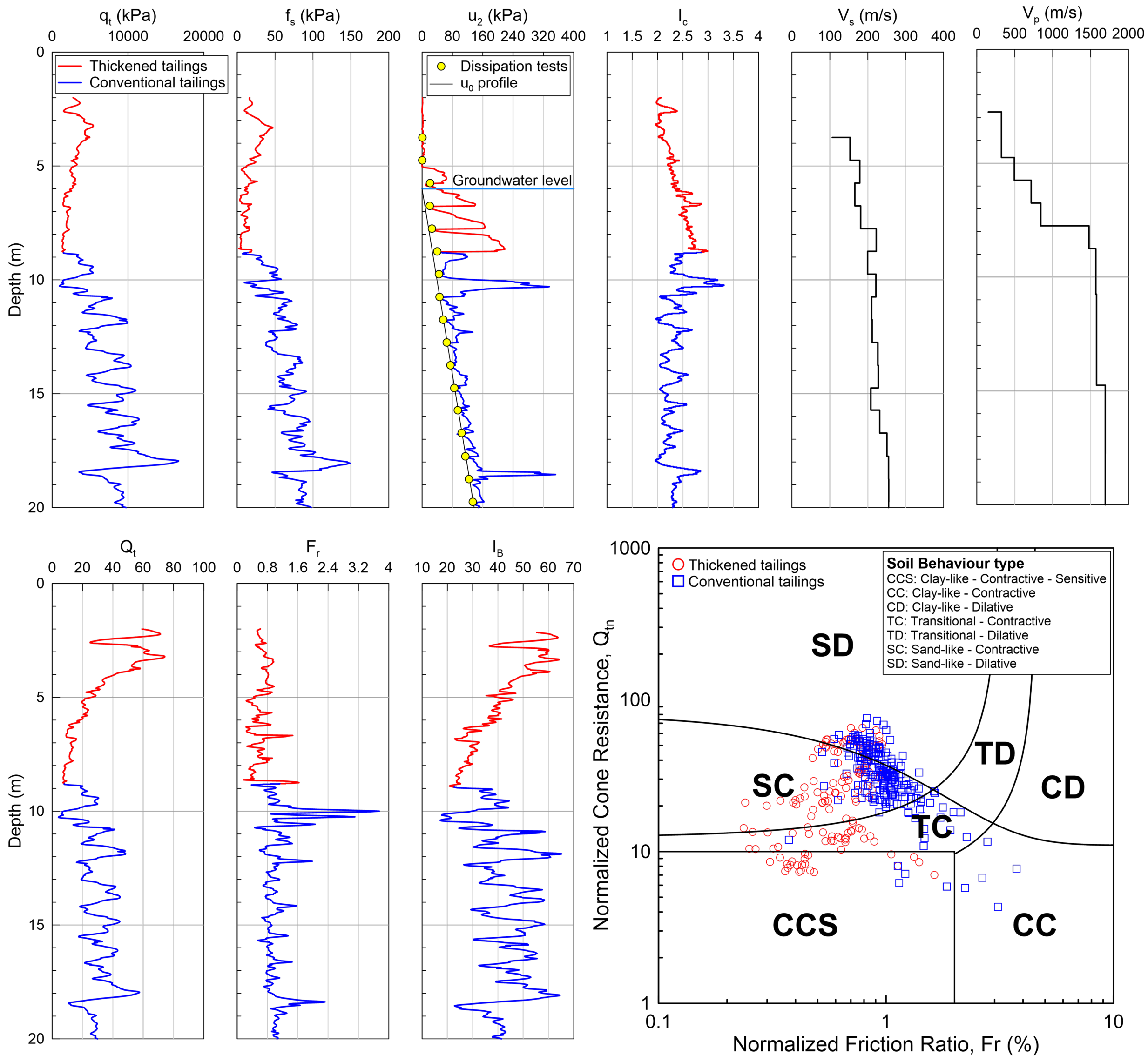

FIG. 4. Variation of q_t, f_s, u_2, I_c, V_s, V_p, Q, F_r, and I_B; for CPTu2 pushed at the standard penetration rate of 2 cm/s. The CPTu data is also shown on the SBTn chart proposed by Robertson (2016)

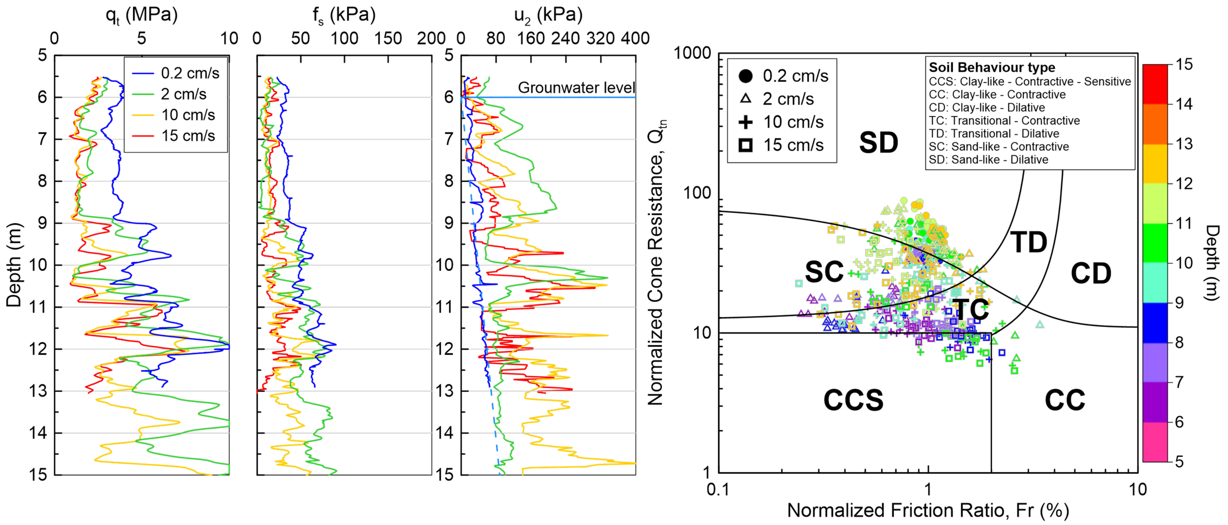

FIG. 5. Variation of q_t, f_s and u_2 for CPTus pushed at 0.2 cm/s, 2 cm/s, 10 cm/s, and 15 cm/s. The CPTu data is also plotted on the SBTn chart proposed by Robertson (2016) for illustrative purposes.

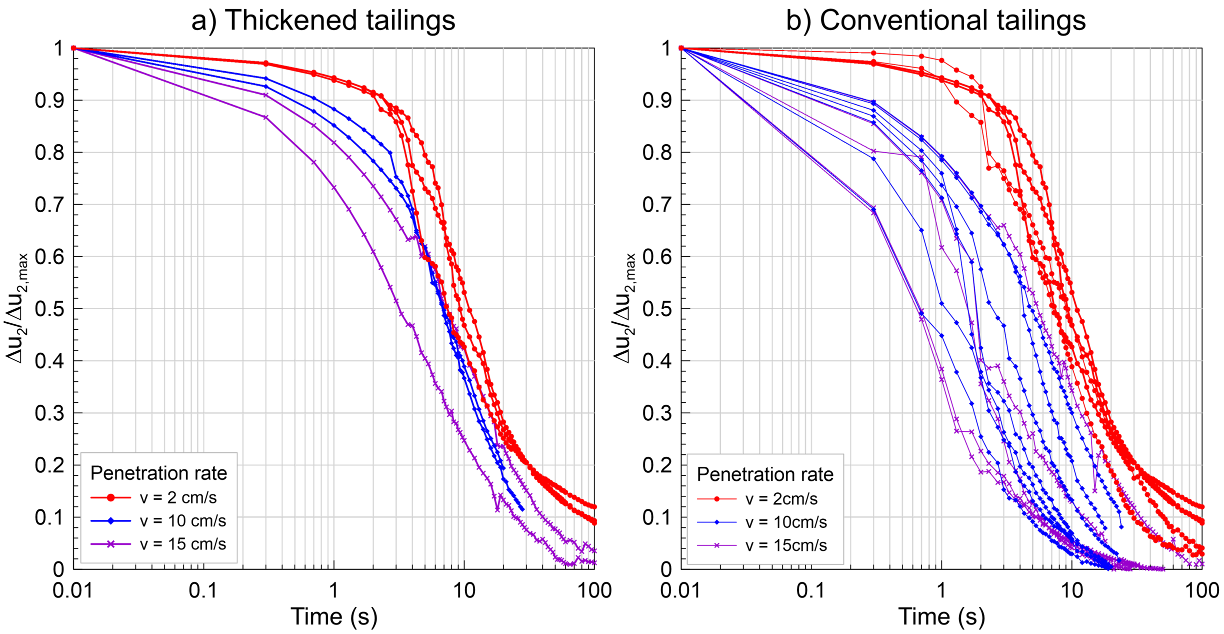

FIG. 6. Normalized excess pore pressure evolution from dissipation tests performed at CPTus pushed at 2cm/s, 10 cm/s, and 15 cm/s. Responses are shown for a) thickened tailings and b) conventional tailings.

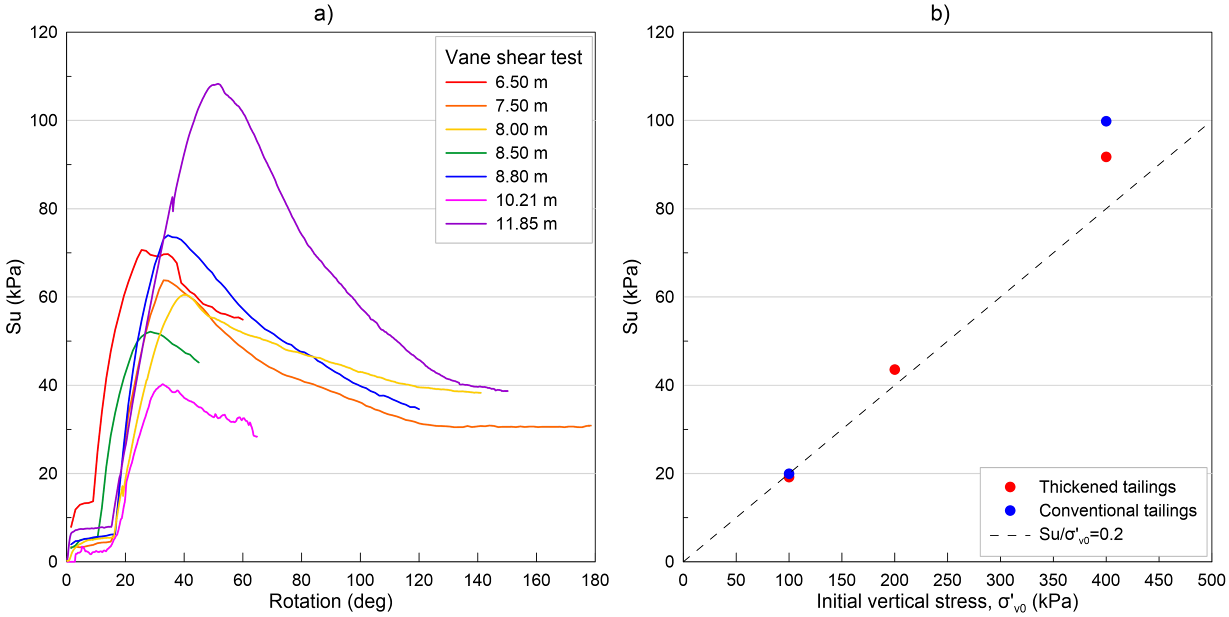

FIG. 7. (a) Responses from vane shear testing (VST). (b) Estimation of peak strength undrained ratio (Su/σ'_v) from undrained triaxial tests

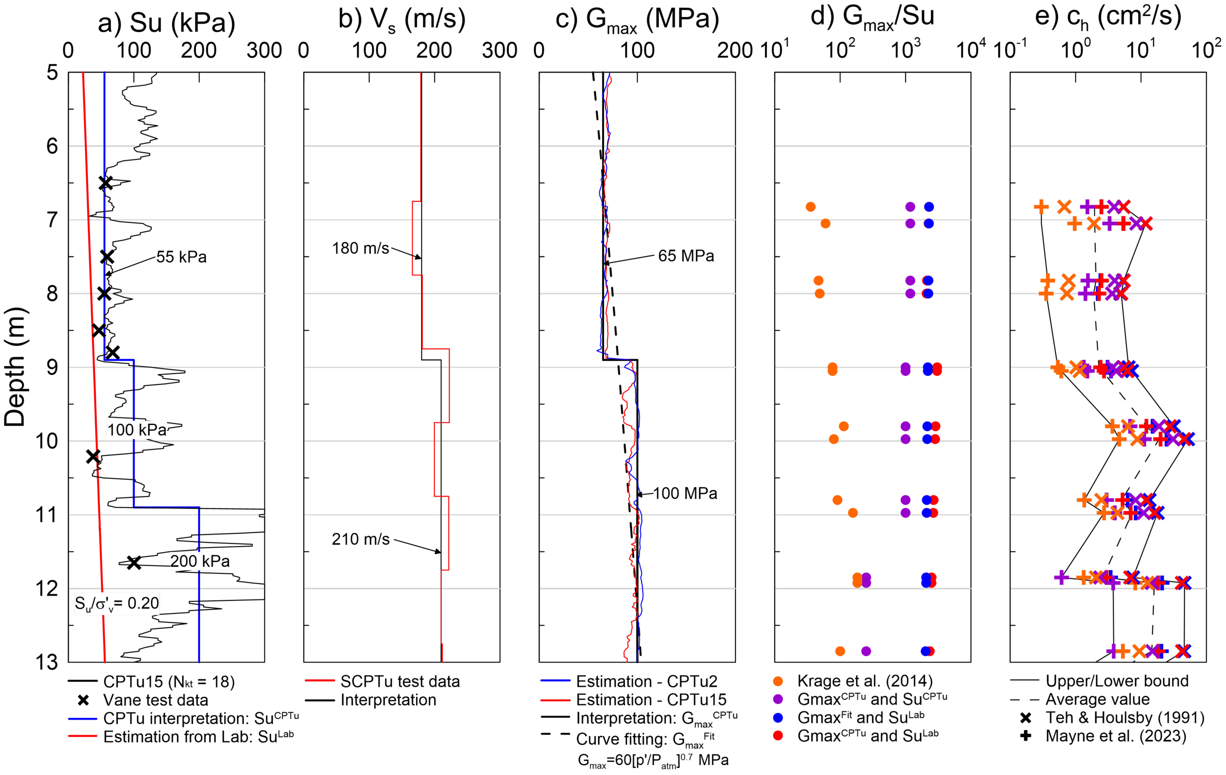

FIG. 8. Variation of (a)Su, (b) V_s, (c) G_{max}, (d) G_{max}/Su, (e) c_h versus depth. See the text for additional details.

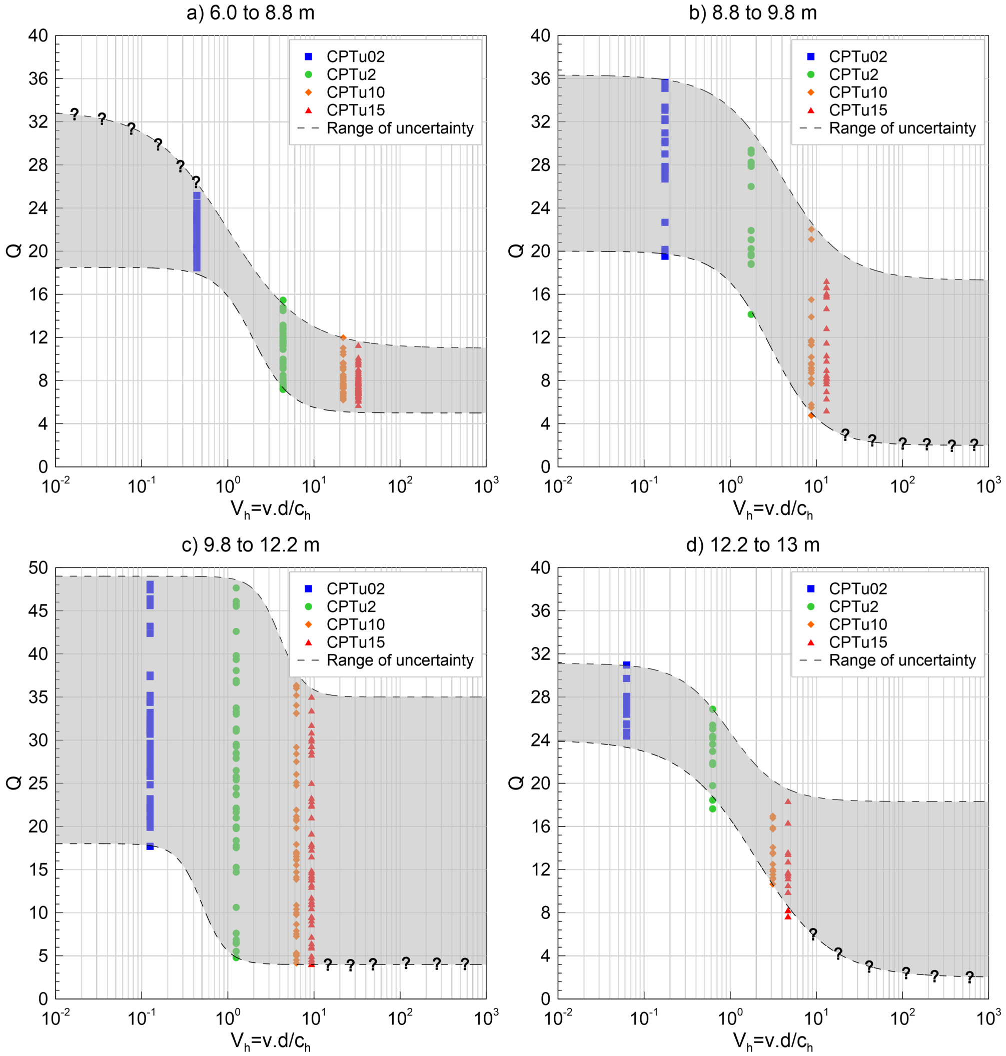

FIG. 9. Range of potential backbone rate effect curves for (a) thickened tailings between 6.0 - 6.8 m, and conventional tailings between (b) 8.8 - 9.8 m, (c) 9.8 - 12.8 m, and (d) 12.2 - 13.0 m.

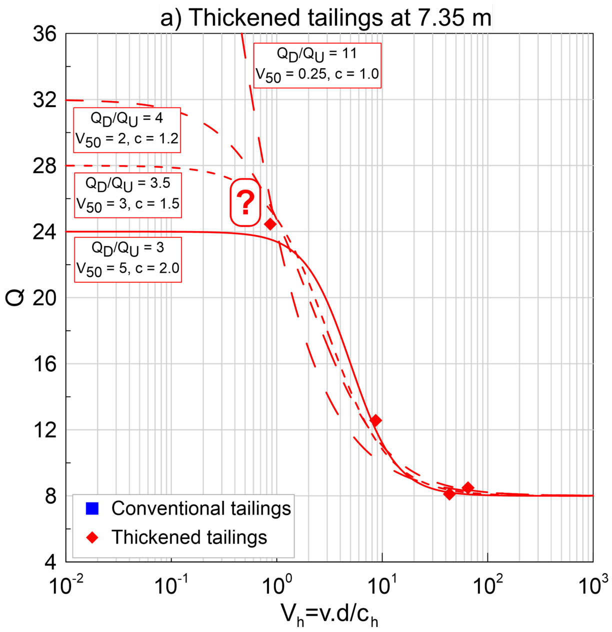

FIG. 10. Plausible backbone rate effect curves for (a) thickened tailings at 7.35 m, and (b) conventional tailings at 12.6 m. The different curves are fitted to the field data using the functional form from DeJong et al. (2012)

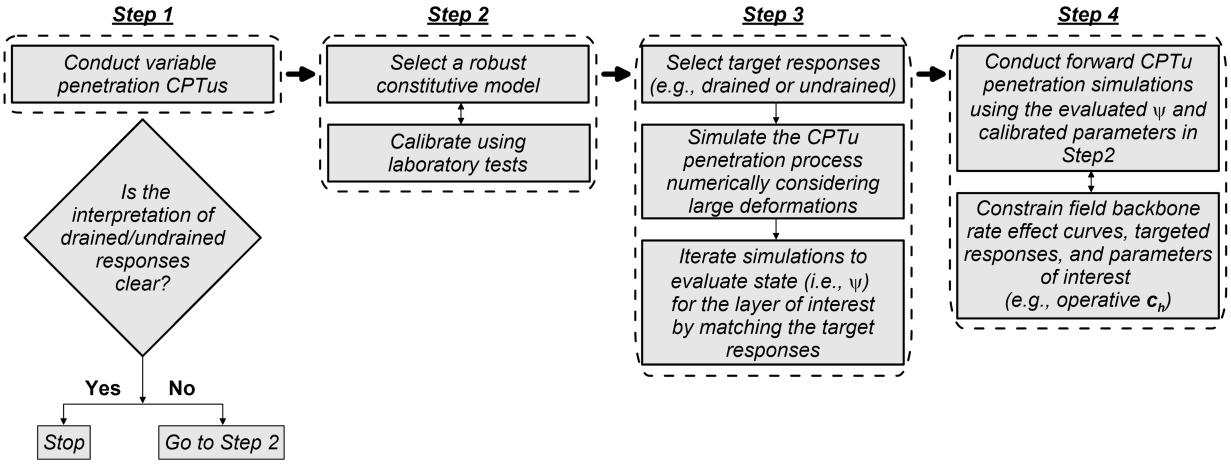

FIG. 11. General framework to interpret variable penetration rate CPTus

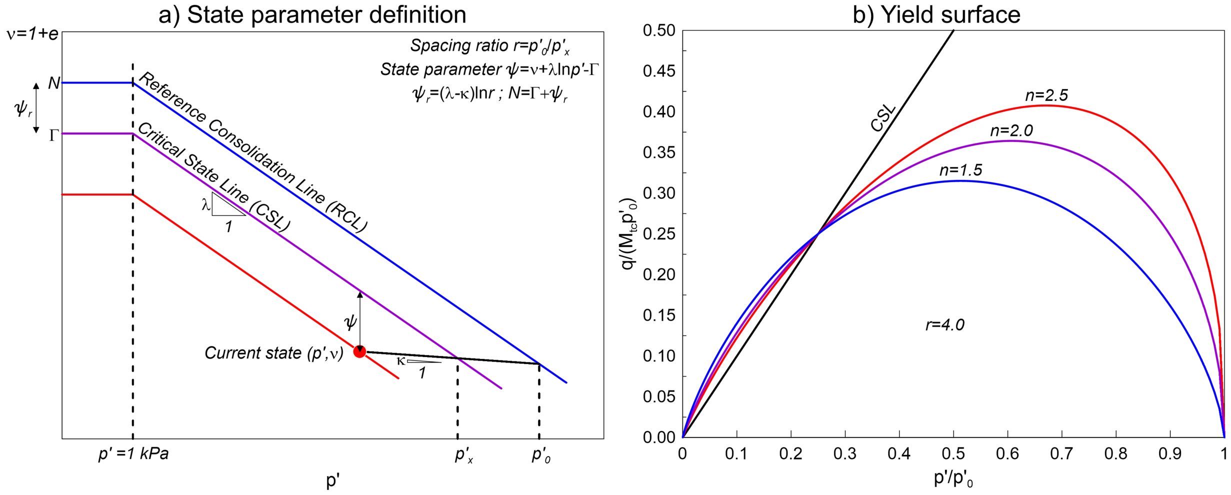

FIG. 12. Clay and Sand Model (CASM) ingredients (a) features in the p'-e space, (b) yield surface shape and variation. Additional details are discussed in the text and electronic supplement.

a) Thickened tailings

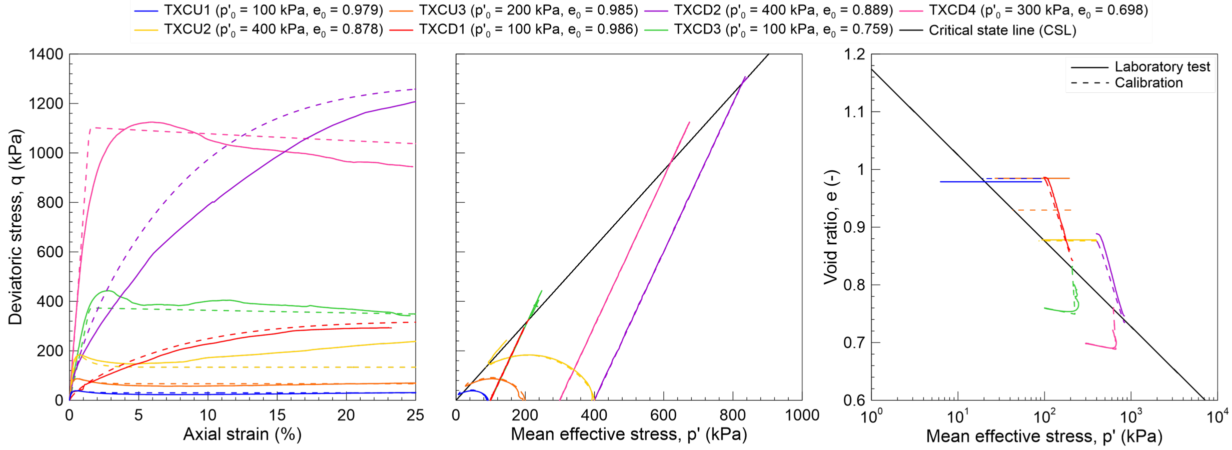

b) Conventional tailings

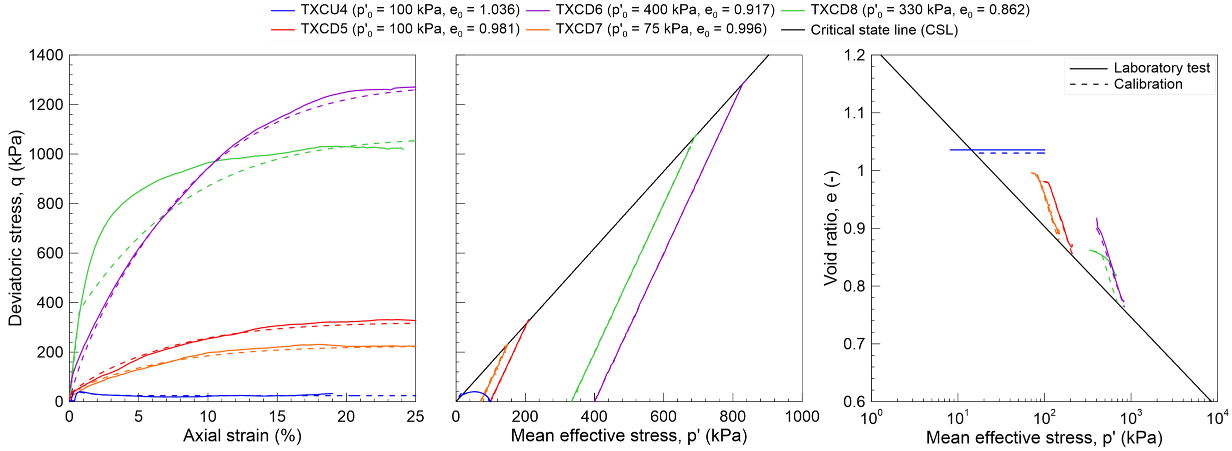

FIG. 13. Comparisons of numerical responses obtained from CASM and experimental responses for (a) thickened tailings, (b) conventional tailings

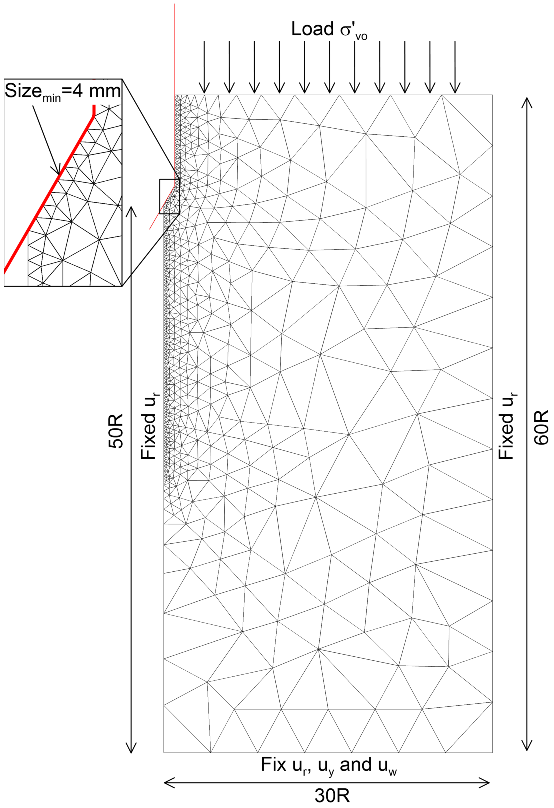

FIG. 14. Mesh discretization and boundary conditions for the G-PFEM based CPTu penetration simulations

a) Mean effective stress

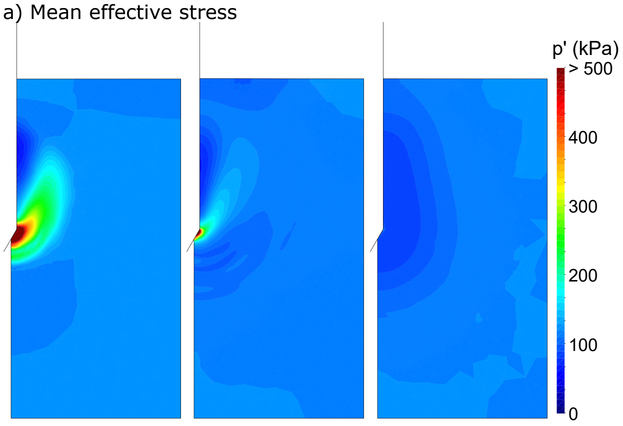

b) Deviatoric stress

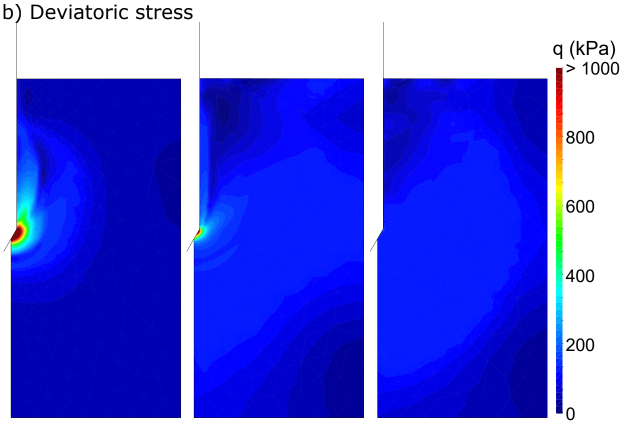

c) Excess pore pressure

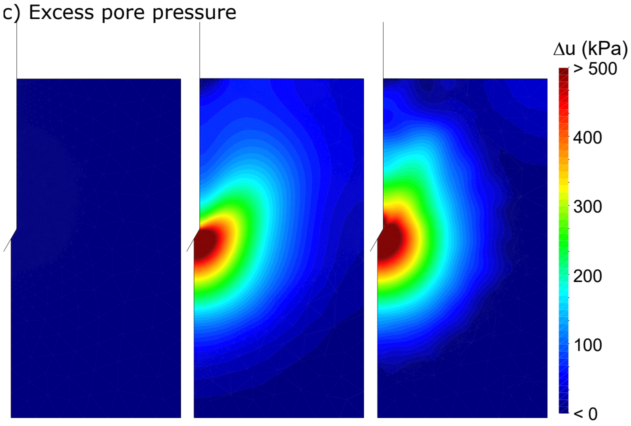

FIG. 15. Distribution of (a) p', (b) q, and (c) excess pore pressure, Δu (bottom) at the end of penetration. The left, middle, and right columns correspond to drained, partially drained, and undrained responses, respectively

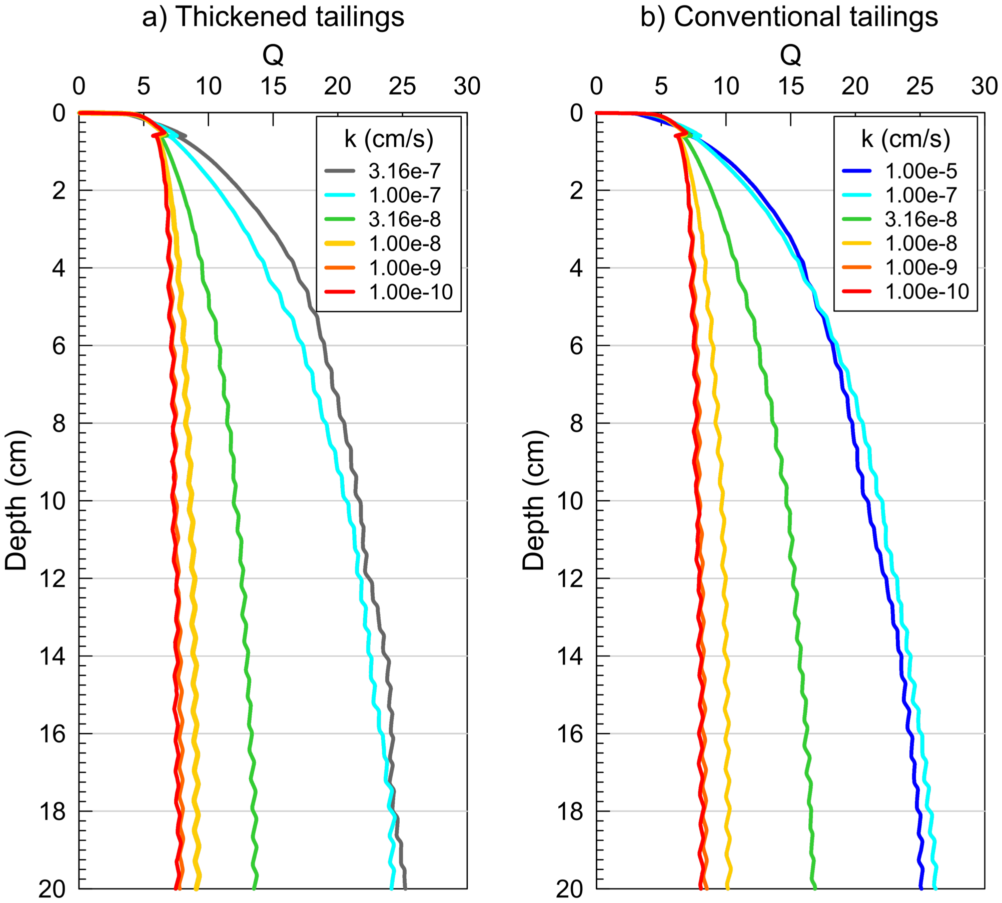

FIG. 16. Variation of Q versus depth obtained from PFEM-based CPTu penetration simulations for (a) thickened tailings and (b) conventional tailings considering different k

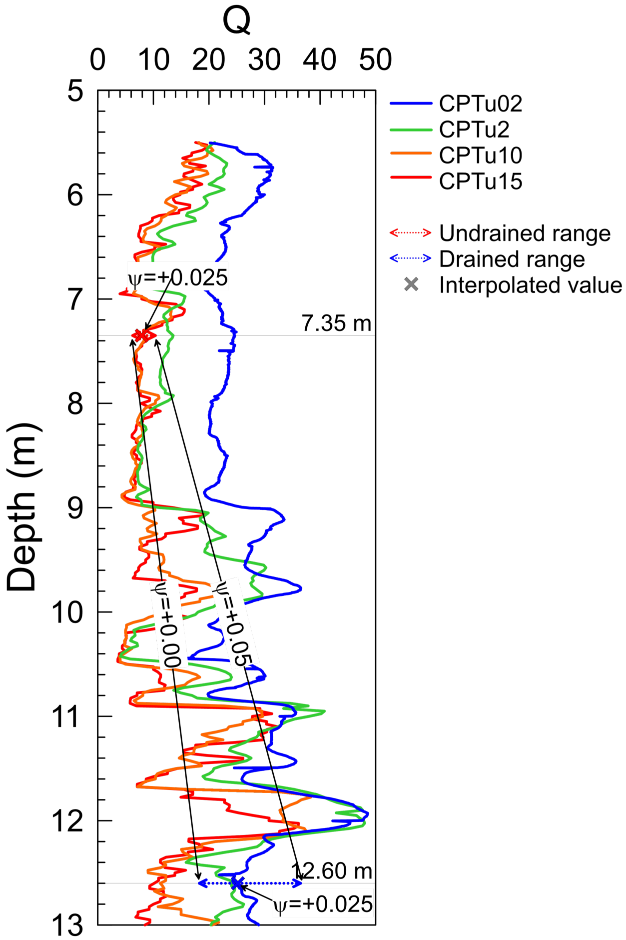

FIG. 17. Illustration of the interpolation procedure to estimate ψ. The horizontal arrows at 7.35 m and 12.60 m represent the range of responses for $\psi = 0.0 - 0.05$ used to inform the next iteration with $\psi = 0.025$

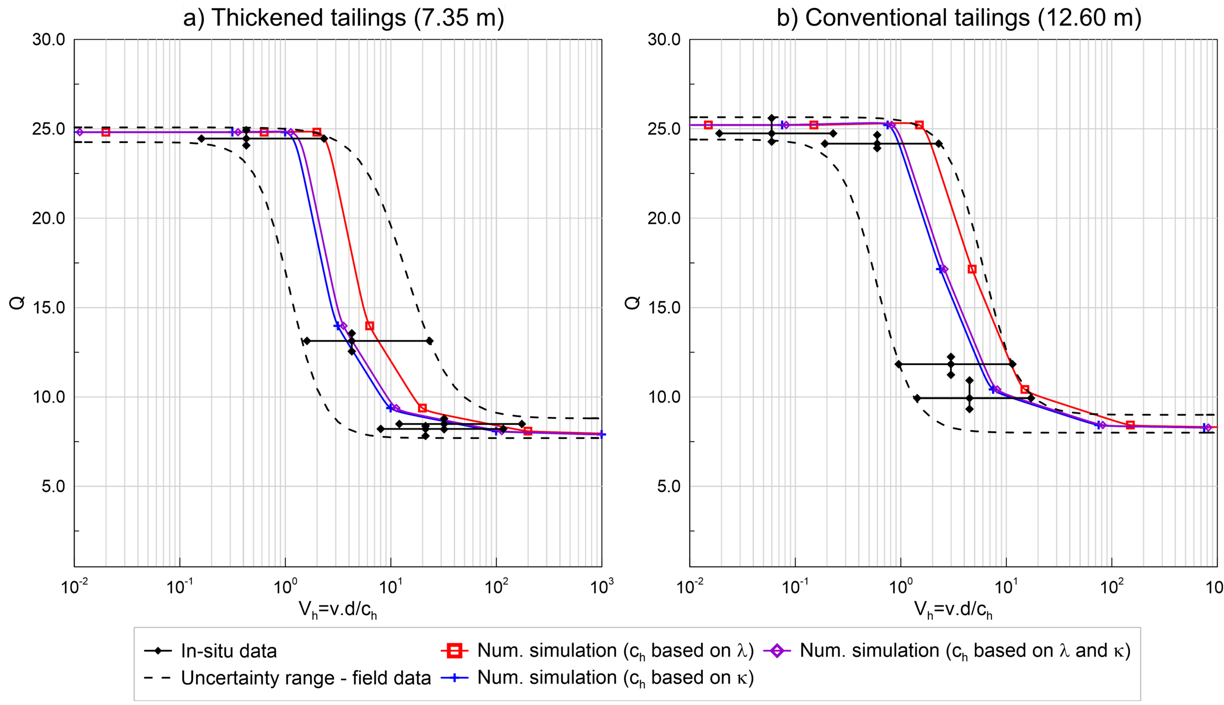

FIG. 18. **Constraining of field-based backbone rate effect curves by using PFEM-based numerical simulations. Notice the narrower range obtained from numerical simulations. Results shown for (a) thickened tailings at 7.35 m and (b) conventional tailings at 12.60 m.**